

Environment assisted superballistic scaling of conductance

Madhumita Saha,^{1,*} Bijay Kumar Agarwalla,^{1,†} Manas Kulkarni,^{2,‡} and Archak Purkayastha^{3,4,§}

¹*Department of Physics, Indian Institute of Science Education and Research Pune,
Dr. Homi Bhabha Road, Ward No. 8, NCL Colony, Pashan, Pune, Maharashtra 411008, India*

²*International Centre for Theoretical Sciences, Tata Institute of Fundamental Research, Bangalore 560089, India*

³*School of Physics, Trinity College Dublin, College Green, Dublin 2, Ireland*

⁴*Centre for complex quantum systems, Aarhus University, Nordre Ringgade 1, 8000 Aarhus C, Denmark*

(Dated: August 9, 2022)

We find that, in the presence of weak incoherent effects from surrounding environments, the zero temperature conductance of nearest neighbour tight-binding chains exhibits a counter-intuitive power-law growth with system length at band-edges, indicating superballistic scaling. This fascinating environment assisted superballistic scaling of conductance occurs over a finite but extended regime of system lengths. This scaling regime can be systematically expanded by decreasing the coupling to the surrounding environments. There is no corresponding analog of this behavior for isolated systems. This superballistic scaling stems from an intricate interplay of incoherent effects from surrounding environments and exceptional points of the system's transfer matrix that occur at every band-edge.

Introduction – The resistance of a normal metal wire is proportional to its length, indicating diffusive transport. As a result, the metal's resistivity, given by resistance per unit length per unit cross-sectional area, is well-defined. Deviation from this diffusive behavior, which leads to ill-defined resistivity, can be seen in a variety of situations, particularly in low-dimensional systems, and has been of great research interest [1–8]. Even outside of the diffusive regime, resistance generically increases with system length. The main exception is that of perfectly ballistic transport where resistance does not scale with system length. Such perfectly ballistic transport is of great benefit in experiments, for example, in superconducting circuits, to build quantum devices.

In this letter, we demonstrate the possibility of behavior different from all of the above: resistance of a wire can decay as power-law with its size, over a finite but large regime of system lengths. In other words, there exists a regime in which conductance, or the inverse of resistance, can increase as a power-law with system length, thereby exhibiting superballistic scaling. This rather counter-intuitive behavior occurs at zero temperature at the band-edges of nearest neighbor tight-binding chains, assisted by weak incoherent effects from the surrounding environments. The regime exhibiting superballistic scaling can be systematically expanded by weakening the system's coupling to its surrounding environments without completely isolating it from them.

We find this intriguing behavior by combining concepts from quantum chemistry and mesoscopic physics with those from non-Hermitian physics. The surrounding environments are modelled by Büttiker voltage probes, as commonly done [9–25]. We show that the superballis-

tic scaling of conductance at every band-edge arises from an interplay of the incoherent effects from the Büttiker probes and exceptional points (EPs) of the system's transfer matrix that occurs at every band-edge [26]. The transfer matrix is a non-Hermitian matrix that appears in scattering theory. It plays a fundamental role in determining the band structure of the system and its transport properties [27–29]. To our knowledge, the role of non-Hermitian properties of the transfer matrix on environment assisted transport has remained unexplored, despite the later being investigated both theoretically and experimentally [23, 30–37].

It is worth mentioning that the term ‘superballistic’ has been used in various separate contexts. In some experiments, conductance larger than the maximum conductance of free electrons has been termed superballistic [38–40]. In a separate set of works, faster-than-ballistic spread of an initially localized wavepacket has been explored both theoretically and experimentally [41–43]. However, to our knowledge, the superballistic scaling of conductance with system length has not been reported before. Unlike the spread of an initially localized wavepacket, this feature crucially requires presence of incoherent effects from surrounding environments and therefore cannot be seen in an isolated system.

Lattice chain with Büttiker voltage probes– We consider a nearest neighbour tight-binding lattice chain consisting of N sites. For simplicity, we consider the single-band Hamiltonian given by $\hat{H}_C = \sum_{n=1}^{N-1} (\hat{c}_n^\dagger \hat{c}_{n+1} + \hat{c}_{n+1}^\dagger \hat{c}_n)$, where \hat{c}_n is the fermionic annihilation operator at the n -th site, and we have set the hopping parameter to 1, which therefore sets our energy scale. All our main results can be carried over to multi-band cases with periodic on-site potentials also. This chain is attached to a source bath with chemical potential μ_L at the left end, i.e, at first site, and a drain bath with chemical potential μ_R at the right end, i.e, at N -th site. The chemical potential difference between the source and the

* madhumita.saha@acads.iiserpune.ac.in

† bijay@iiserpune.ac.in

‡ manas.kulkarni@icts.res.in

§ archak.p@phys.au.dk

drain drives a current through the lattice chain. To model incoherent effects coming from surrounding environments which does not directly take part in transport (i.e., zero net current between each site of the lattice system and the probes), we further connect to each lattice site of the chain to a Büttiker voltage probe. These are baths similar to the source and drain baths, except that their chemical potentials, $\{\mu_n\}$, are such that there is no average particle current into each of them. The temperature of all the baths are considered same, given by inverse temperature β . The microscopic Hamiltonian \hat{H} for this whole set-up can be written as, $\hat{H} = \hat{H}_C + \hat{H}_L + \hat{H}_R + \sum_{n=1}^N \hat{H}_{P_n} + \hat{H}_{CL} + \hat{H}_{CR} + \sum_{n=1}^N \hat{H}_{CP}^{(n)}$, where \hat{H}_C is the Hamiltonian of the tight-binding chain (central system), \hat{H}_L is the Hamiltonian of the left bath (source), \hat{H}_R is the Hamiltonian of the right bath (drain), \hat{H}_{P_n} is the Hamiltonian of the probe attached to the n -th site of the system, \hat{H}_{CL} , \hat{H}_{CR} and $\hat{H}_{CP}^{(n)}$ are the Hamiltonians which describe the coupling of central system with source, drain, and n -th probe respectively. Each bath is modelled via an infinite number of fermionic modes, and the system bath couplings are taken bilinear, such that \hat{H} is quadratic, number conserving Hamiltonian. A schematic of our entire setup is shown in Fig. (1).

In the non-equilibrium steady state (NESS), there is flow of current from source to drain. Note that, by construction, there is no average current flowing into the probe baths. The presence of these probe baths, however, crucially alters the transport properties. To see this, we describe the NESS of the system via the non-equilibrium Green's function (NEGF) technique. The retarded Green's function of the system in presence of the baths is given by $G(\omega) = [\omega \mathbb{I} - H_C - \Sigma_L(\omega) - \Sigma_R(\omega) - \sum_{n=1}^N \Sigma_{P_n}(\omega)]^{-1}$ where \mathbb{I} is the $N \times N$ identity matrix, H_C is the $N \times N$ single particle Hamiltonian corresponding to \hat{H}_C , and $\Sigma_L(\omega)$, $\Sigma_R(\omega)$, $\Sigma_{P_n}(\omega)$ are the retarded self-energy matrices of the left, right and probe baths respectively. The effect of each bath is encoded in their corresponding self-energy matrices. For a bath attached to n -th site of the system, only the corresponding diagonal element of the self-energy matrix is non-zero, while all other elements of the matrix are zero. For simplicity, here, we choose $[\Sigma_L(\omega)]_{11} = -i\tau/2$, $[\Sigma_R(\omega)]_{NN} = -i\tau/2$, and $[\Sigma_{P_n}(\omega)]_{nn} = -i\tau_p/2$ which corresponds to the so-called wide-band limit. Here τ_p gives the effective strength of coupling to probe baths (taken to be same for all probe baths), and τ gives the same for the left and the right baths.

We are interested in zero temperature ($\beta \rightarrow \infty$), linear response regime. We set, $\mu_R = \epsilon_F$, $\mu_L = \epsilon_F + \delta\mu$, $\mu_n = \epsilon_F + \delta\mu_n$, where ϵ_F is the Fermi energy. In this multi-terminal setting along with the constraint that there is no average current into the probe baths, the conductance

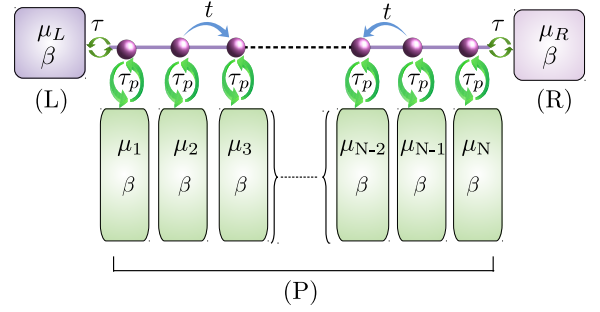


FIG. 1. A schematic of our set-up showing a tight-binding lattice with hopping parameter t subjected to left bath (L), right bath (R) and voltage probes (P), all of which are at the same inverse temperature β . The left and right baths are coupled with strength τ , while the probes are coupled with strength τ_p . The chemical potential of the probes μ_n , $n = 1, 2, \dots, N$ are determined by demanding the zero particle current between n -th site and n -th probe.

is given by the Landauer-Buttiker theory as [44]

$$\mathcal{G}(\epsilon_F) = \tau^2 |G_{1N}(\epsilon_F)|^2 + \tau^2 \tau_p \sum_{n,j=1}^N |G_{Nn}(\epsilon_F)|^2 \mathcal{W}_{nj}^{-1}(\epsilon_F) |G_{j1}(\epsilon_F)|^2. \quad (1)$$

Here the elements of the $N \times N$ matrix $\mathcal{W}(\epsilon_F)$ are

$$\mathcal{W}_{nj} = -\tau_p |G_{nj}|^2, \quad \forall n \neq j$$

$$\mathcal{W}_{nn} = \tau (|G_{n1}|^2 + |G_{nN}|^2) + \tau_p \sum_{j \neq n} |G_{nj}|^2, \quad (2)$$

where we have suppressed the argument ϵ_F for brevity. The above equations show that, knowing the retarded NEGF, the conductance in presence of the probes can be obtained. In absence of the probes [i.e., setting $\tau_p = 0$ in Eq. (S9)], the conductance is given by $\mathcal{G}^0(\epsilon_F) = \tau^2 |G_{1N}^0(\epsilon_F)|^2$, where $G^0(\epsilon_F)$ is the retarded NEGF in absence of the probes.

NEGF and transfer matrix — For our chosen system Hamiltonian, H_C is a tridiagonal matrix with all its non-zero off-diagonal elements being equal to 1, and diagonal elements being zero. Hence, the retarded Green's function $G(\omega)$ is the inverse of a tridiagonal matrix. Using properties of such tridiagonal matrices, the elements of $G(\omega)$ can be written as [44]

$$G_{\ell j}(\omega) = (-1)^{\ell+j} \frac{\Delta_{1,\ell-1}(\omega) \Delta_{N-j,N}(\omega)}{\Delta_{1,N}(\omega)}, \quad (3)$$

where $\Delta_{1,\ell-1}(\omega)$, $\Delta_{N-j,N}(\omega)$, $\Delta_{1,N}(\omega)$ satisfy the follow-

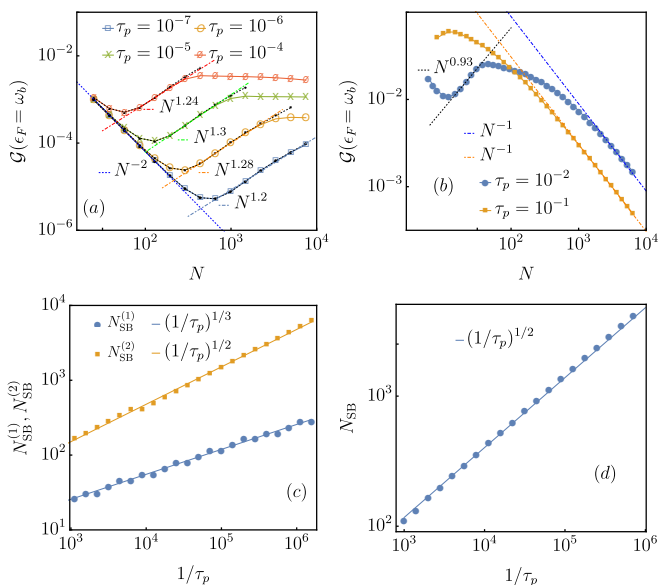


FIG. 2. (a) Behavior of conductance at band-edges $\epsilon_F = \omega_b$ vs system length N for small values of τ_p . The black dots show approximate result obtained on replacing $G(\omega_b)$ by $G^0(\omega_b)$ (i.e., without the probes) in Eqs. (S9) and (S8). We see a clear evidence of sub-diffusive to superballistic crossover. (b) Similar plots but at larger values of τ_p which captures the eventual crossover to conventional diffusive regime at large N . (c) The scaling of the start (end) of the superballistic regime $N_{\text{SB}}^{(1)}$ ($N_{\text{SB}}^{(2)}$) with τ_p^{-1} . (d) The scaling of the size of the superballistic scaling regime $N_{\text{SB}} = N_{\text{SB}}^{(2)} - N_{\text{SB}}^{(1)}$ with τ_p^{-1} . This plot clearly shows that the superballistic scaling regime expands on decreasing τ_p . In all cases, both band-edges $\omega_b = \pm 2$ show identical behavior.

ing equations

$$\begin{aligned} \begin{pmatrix} \Delta_{1,N}(\omega) \\ \Delta_{1,N-1}(\omega) \end{pmatrix} &= \begin{pmatrix} 1 & \frac{i\tau}{2} \\ 0 & 1 \end{pmatrix} [\mathbf{T}(\omega)]^N \begin{pmatrix} 1 \\ -\frac{i\tau}{2} \end{pmatrix}, \\ \begin{pmatrix} \Delta_{1,\ell-1}(\omega) \\ \Delta_{1,\ell-2}(\omega) \end{pmatrix} &= \begin{pmatrix} 1 & \frac{i\tau}{2} \\ 0 & 1 \end{pmatrix} [\mathbf{T}(\omega)]^{\ell-1} \begin{pmatrix} 1 \\ 0 \end{pmatrix}, \\ \begin{pmatrix} \Delta_{N-j,N}(\omega) \\ \Delta_{N-j-1,N}(\omega) \end{pmatrix} &= [\mathbf{T}(\omega)]^{N-j} \begin{pmatrix} 1 \\ -\frac{i\tau}{2} \end{pmatrix}. \end{aligned} \quad (4)$$

In above $\mathbf{T}(\omega)$ is a 2×2 matrix given by

$$\mathbf{T}(\omega) = \mathbf{T}^0(\omega) + \frac{i\tau_p}{4} (\mathbb{I}_2 + \sigma_z), \quad (5)$$

where $\mathbf{T}^0(\omega) = \frac{\omega}{2} (\mathbb{I}_2 + \sigma_z) - i\sigma_y$ is the transfer matrix of the tight-binding chain, \mathbb{I}_2 is 2×2 identity matrix and $\sigma_{x,y,z}$ are the Pauli matrices. The transfer matrix determines the band structure of the chain in the thermodynamic limit in absence of the baths via the relation $\text{Tr}[\mathbf{T}^0(\omega)] = 2 \cos k$, where k is the Bloch wave-vector [26–29]. This, in our simple single-band setting, gives the standard dispersion relation $\omega = 2 \cos k$. The band-edges correspond to $k = 0, \pm\pi$, where $\omega \equiv \omega_b = \pm 2$.

It is clear that the nature of $\mathbf{T}(\omega)$ controls the system size scaling of various elements of the retarded NEGF.

The determinants of both $\mathbf{T}(\omega)$ and $\mathbf{T}^0(\omega)$ are 1. So, in complete generality, their eigenvalues can be written in the form $\lambda_{\pm} = e^{\pm(\kappa_1 + i\kappa_2)}$, with $\kappa_1, \kappa_2 \geq 0$, which ensures product of eigenvalues is 1. For $\mathbf{T}^0(\omega)$ it is easy to check that at least one of κ_1, κ_2 is zero for all ω . For $|\omega| < 2$, the eigenvalues of $\mathbf{T}^0(\omega)$ are complex conjugates of each other, which implies $\kappa_1 = 0$. For $|\omega| > 2$, the eigenvalues are real, i.e., $\kappa_2 = 0$, while for $|\omega| = 2$, i.e., at the band edges, both $\kappa_1, \kappa_2 = 0$, thereby implying the existence of a single eigenvalue. This means for $\omega = \omega_b = \pm 2$, $\mathbf{T}^0(\omega_b)$ is not diagonalizable. The band-edges therefore correspond to the EPs of the transfer matrix. As has been recently shown [26], this behavior is a consequence of an antilinear symmetry of transfer matrices of nearest-neighbour tight-binding chains, and holds in general even for multi-band cases. As a consequence, in absence of the probes, conductance shows a universal sub-diffusive scaling $\mathcal{G}^0(\omega_b) \sim N^{-2}$ at every band-edge [26]. In the presence of the probes [i.e., considering the last term in Eq. (5)], the transport properties at these band edges get significantly impacted which is the central focus of this work.

The presence of the probes makes $\kappa_1 > 0 \forall \omega$ thereby implying the lack of antilinear symmetry, and making $\mathbf{T}(\omega)$ always diagonalizable, as can be easily confirmed by direct calculation. Consequently, from Eqs. (S24) and (3), it can be shown that, for $|\ell - j|$ large, $|G_{\ell j}(\omega)|^2 \sim e^{-|\ell - j|/\xi}$, with $\xi^{-1} = 2\kappa_1 = 2 \log |\lambda_+|$ [44] where we recall that λ_+ is one of the eigenvalues of $\mathbf{T}(\omega)$. Whenever this is the case, the conductance in Eq. (S9) gives diffusive scaling $\mathcal{G}(\omega) \sim N^{-1}$, for $N \gg \xi$, as has been shown in seminal work [20]. This holds for all values of ω . Hence, in presence of probes, at large enough system sizes, we always get normal diffusive behavior. Here, we are interested in the regime, $N \lesssim \xi$. It is in this regime that we find the superballistic scaling of conductance at band-edges, as we show below.

Numerical results — We now present our main numerical results. In Fig. 2(a), we show plots of conductance with system length at band-edge, i.e, aligning the Fermi energy with the band-edge of the lattice chain ($\epsilon_F = \omega_b$), for various small values of probe strength τ_p . For small N , we clearly see a remnant of the sub-diffusive scaling, $\mathcal{G}(\omega_b) \sim N^{-2}$ expected in absence of probes. After this, we find the surprising superballistic scaling, $\mathcal{G}(\omega_b) \sim N^{\phi}$, $\phi > 0$ for a finite regime in system length. The exponent ϕ is non-universal, $\phi \gtrsim 1.2$, depending weakly on τ_p . Importantly, the superballistic scaling regime expands as τ_p is reduced. Beyond the superballistic scaling regime, the conductance starts saturating with system length, eventually decaying as we increase the system length further. Although not seen in our numerics for small τ_p up to the largest accessible N , we expect this slow decay with system length to eventually lead to standard diffusive behavior $\mathcal{G}(\omega_b) \sim N^{-1}$. This is captured for sufficiently large values of τ_p in Fig. 2(b).

To further analyze the superballistic scaling regime, we extract from our numerics the onset and the termination

of this regime. These correspond to the minimum and the maximum of the plots in Fig. 2(a), respectively. In Fig. 2(c), we plot the starting (ending) system size of superballistic scaling regime, $N_{\text{SB}}^{(1)}$ ($N_{\text{SB}}^{(2)}$), as a function of τ_p^{-1} . We find that $N_{\text{SB}}^{(1)} \sim \tau_p^{-1/3}$ and $N_{\text{SB}}^{(2)} \sim \tau_p^{-1/2}$. For $\tau_p \ll 1$, we have $\tau_p^{-1/3} \ll \tau_p^{-1/2}$, which shows that the superballistic scaling regime can be enhanced by reducing τ_p . The size of this superballistic regime, $N_{\text{SB}} = N_{\text{SB}}^{(2)} - N_{\text{SB}}^{(1)}$ therefore scales as $N_{\text{SB}} \sim \tau_p^{-1/2}$, for small τ_p , as shown in Fig. 2(d). This counter-intuitive behavior of conductance at the band-edges is our main result. Away from band-edges, no superballistic scaling is seen. For $|\epsilon_F| < 2$, i.e, Fermi energy within the system band, there is smooth ballistic to diffusive crossover as a function of system length. For $|\epsilon_F| > 2$, i.e, Fermi energy outside the system band, transport becomes diffusive even at very small values of τ_p . The cases away from band-edges have been investigated in several previous works [20, 36, 45].

Analytical viewpoint — To analytically understand our numerical results, we begin by calculating the magnitude of eigenvalues of $\mathbf{T}(\omega_b)$ to the leading order in τ_p . At $\omega = \omega_b$, the magnitude of eigenvalues can be shown to be $|\lambda_{\pm}| \simeq 1 \pm \sqrt{\tau_p}$. This leads to $\xi^{-1} = 2 \log |\lambda_{+}| \simeq 2\sqrt{\tau_p}$ [44]. We know that for $N \gg \xi$, conductance scales diffusively. So, the superballistic scaling should end when $N \sim \xi$, which gives the scaling of $N_{\text{SB}}^{(2)}$ as $N_{\text{SB}}^{(2)} \sim \tau_p^{-1/2}$, where we recall that $N_{\text{SB}}^{(2)}$ corresponds to the ending of the superballistic regime. This is exactly as numerically seen in Fig. 2(c).

For small τ_p and $N \ll N_{\text{SB}}^{(2)}$, following Eq.(5), the leading order behavior should be captured by using $\mathbf{T}(\omega_b) \simeq \mathbf{T}^0(\omega_b)$. This is same as using Eqs.(S9), (S8), with $G(\epsilon_F)$ replaced by the retarded NEGF in absence of probes, $G^0(\epsilon_F)$. This approximation can also be justified using a more careful, order-by-order perturbation in τ_p . Conductance calculated in this approximation is shown by the black dots in Fig. 2. Indeed they overlap with the exact results in the entire sub-diffusive and the superballistic regimes. Next, to understand the behavior of $N_{\text{SB}}^{(1)}$ with τ_p , we look at the condition for observing the sub-diffusive scaling. Clearly, this is seen in the regime where the effect of the probes is negligible. So, we calculate the expression for conductance up to the lowest order in τ_p . Since the second term in Eq. (S9) is explicitly proportional to τ_p , in calculating all required matrix elements for that term, we simply set τ_p to zero. From Eq. (S8), we see that this makes $\mathcal{W}(\epsilon_F)$ diagonal, which leads to

$$\mathcal{G} = \tau^2 |G_{1N}^0|^2 + \tau\tau_p \sum_{\ell=1}^N \frac{|G_{\ell N}^0|^2 |G_{1\ell}^0|^2}{|G_{1\ell}^0|^2 + |G_{\ell N}^0|^2} + \mathcal{O}(\tau_p^2), \quad (6)$$

where we have once again suppressed the argument ϵ_F for brevity. Due to transfer matrix EP at $\epsilon_F = \omega_b$, it can be checked that the second term in above expression diverges as N , while the first term decays as N^{-2} [44]. Clearly, $N_{\text{SB}}^{(1)}$, which gives the end of the sub-

diffusive regime and the beginning of the superballistic regime, must correspond to the case where the two terms in Eq. (6) are comparable, $\tau N_{\text{SB}}^{(1)-2} \sim \tau_p N_{\text{SB}}^{(1)}$. This directly gives $N_{\text{SB}}^{(1)} \sim \tau_p^{-1/3}$, as has been numerically seen in Fig. 2(c). Thus, we conclude that the superballistic scaling comes from the second term in Eq. (S9), in the regime where the EP of the transfer matrix governs its leading behavior. This clearly shows that the surprising superballistic scaling regime comes as an interplay of the transfer matrix EP and weak incoherent effects due to the probes.

Probes versus many-body interaction — The Büttiker probes mimic inelastic scattering processes due to surrounding environments [10, 36, 46, 47]. Another way in which inelastic scattering can originate is via many-body interactions in the system. So, one might naively expect that in absence of the probes, adding many-body interactions in the central system will lead to a similar effect. However, this is not the case here. In absence of the probes, at the lower band-edge, i.e., $\epsilon_F = -2$, particle density in the system, defined as, $\gamma = \sum_{\ell=1}^N \frac{1}{N} \langle c_{\ell}^{\dagger} c_{\ell} \rangle$, decays with N [44]. Due to vanishing particle density at large N , the physics is primarily governed by the single-particle sector even in presence of number conserving many-body interactions. Consequently, the sub-diffusive behavior that is seen in absence of many-body interactions survives even in the presence of number conserving interactions. Analogous statements also hold for the upper band-edge, $\epsilon_F = 2$, with particles replaced by holes. This is in stark contrast with what happens in the presence of probes. Thus, at band-edges, the counter-intuitive effect of the probes cannot be reproduced with only many-body interactions in the central system.

Generalization — Our results above for the single-band nearest neighbour tight-binding chain hold for multi-band cases also. Our analytical understanding shows that the existence of the superballistic scaling regime stems from $\xi^{-1} \propto \sqrt{\tau_p}$ and the first term in Eq. (6) scaling as N^{-2} , while the second term scaling as N . The EP of the system's transfer matrix is responsible for all of these behaviors. There is a transfer matrix EP at every band-edge of any nearest neighbor tight-binding chain, whether single-band or multi-band, and all of these behaviors are the same. As a result, a superballistic scaling regime will be seen in all such cases. For example, in a two-band case, this can be easily explicitly confirmed [44]. Furthermore, while we assumed wide-band baths for simplicity, all of our results are applicable to arbitrary bath spectral functions as long as the probe bath spectral functions are the same and the bath bands encompass the system's spectrum. Our results, however, are not robust to the presence of disorder because Bloch's theorem does not hold and band-edges are ill-defined in that case.

Conclusions and outlook — We show how non-Hermitian properties of the transfer matrix of the nearest neighbour tight-binding chain affect environment assisted

transport, the environment being modelled by Büttiker probes. At every band-edge of the chain, an intricate interplay of transfer matrix EP and weak incoherent effects from probes leads to a power law increase of zero temperature conductance with system length. This fascinating environment assisted superballistic scaling of conductance is seen over a finite regime of system lengths. This regime can be systematically expanded by decreasing the coupling to the environments, without completely decoupling them. This remarkable phenomena has no analog in isolated systems. We believe this intriguing behavior will be of fundamental interest across quantum chemistry, mesoscopic physics, non-Hermitian physics, and statistical physics. It can be expected to have practical implications in nanoscale quantum devices. Future work includes probing the effect of long-range hopping on the superballistic scaling regime. The simultaneous presence of voltage probes and many-body interactions remains a challenging and interesting question.

M. S. acknowledge financial support through National Postdoctoral Fellowship (NPDF), SERB file no. PDF/2020/000992. B. K. A. acknowledges the MATRICS grant (MTR/2020/000472) from SERB, Government of India and the Shastri Indo-Canadian Institute for providing financial support for this research work in the form of a Shastri Institutional Collaborative Research Grant (SICRG). B. K. A. would also like to ac-

knowledge funding from National Mission on Interdisciplinary Cyber-Physical Systems (NM-ICPS) of the Department of Science and Technology, Govt. Of India through the I-HUB Quantum Technology Foundation, Pune INDIA. M.K. would like to acknowledge support from the project 6004-1 of the Indo-French Centre for the Promotion of Advanced Research (IFCPAR), Ramanujan Fellowship (SB/S2/RJN-114/2016), SERB Early Career Research Award (ECR/2018/002085) and SERB Matrics Grant (MTR/2019/001101) from the Science and Engineering Research Board (SERB), Department of Science and Technology, Government of India. MK acknowledges support of the Department of Atomic Energy, Government of India, under Project No. RTI4001. A.P acknowledges funding from the European Union's Horizon 2020 research and innovation programme under the Marie Skłodowska-Curie Grant Agreement No. 890884. A.P also acknowledges funding from the Danish National Research Foundation through the Center of Excellence "CCQ" (Grant agreement no.: DNR156). This research was supported in part by the International Centre for Theoretical Sciences (ICTS) for participating in the program - Physics with Trapped Atoms, Molecules and Ions (code: ICTS/TAMIONS-2022/5). M.K. acknowledges support from the Infosys Foundation International Exchange Program at ICTS.

-
- [1] X. Xu, L. F. C. Pereira, Y. Wang, J. Wu, K. Zhang, X. Zhao, S. Bae, C. Tinh Bui, R. Xie, J. T. L. Thong, B. H. Hong, K. P. Loh, D. Donadio, B. Li, and B. Özyilmaz, *Nature Communications* **5**, 3689 (2014).
- [2] T. Meier, F. Menges, P. Nirmalraj, H. Hölscher, H. Riel, and B. Gotsmann, *Phys. Rev. Lett.* **113**, 060801 (2014).
- [3] A. K. Majee and Z. Aksamija, *Phys. Rev. B* **93**, 235423 (2016).
- [4] Q.-Y. Li, K. Takahashi, and X. Zhang, *Phys. Rev. Lett.* **119**, 179601 (2017).
- [5] D. L. Nika, A. S. Askerov, and A. A. Balandin, *Nano Letters* **12**, 3238 (2012).
- [6] Z. Xu, *Theoretical and Applied Mechanics Letters* **6**, 113 (2016).
- [7] A. Purkayastha, A. Dhar, and M. Kulkarni, *Phys. Rev. B* **96**, 180204 (2017).
- [8] A. Purkayastha, S. Sanyal, A. Dhar, and M. Kulkarni, *Phys. Rev. B* **97**, 174206 (2018).
- [9] M. Büttiker, *Phys. Rev. Lett.* **57**, 1761 (1986).
- [10] J. Maassen, F. Zahid, and H. Guo, *Phys. Rev. B* **80**, 125423 (2009).
- [11] C. J. Cattena, R. A. Bustos-Marín, and H. M. Pastawski, *Phys. Rev. B* **82**, 144201 (2010).
- [12] D. Nozaki, C. Gomes da Rocha, H. M. Pastawski, and G. Cuniberti, *Phys. Rev. B* **85**, 155327 (2012).
- [13] J. Maassen, F. Zahid, and H. Guo, *Phys. Rev. B* **80**, 125423 (2009).
- [14] D. Nozaki, Y. Girard, and K. Yoshizawa, *The Journal of Physical Chemistry C* **112**, 17408 (2008).
- [15] M. Kilgour and D. Segal, *The Journal of Chemical Physics* **144**, 124107 (2016).
- [16] M. Kilgour and D. Segal, *The Journal of Chemical Physics* **143**, 024111 (2015).
- [17] R. Korol, M. Kilgour, and D. Segal, *Computer Physics Communications* **224**, 396 (2018).
- [18] M. Bandyopadhyay and D. Segal, *Phys. Rev. E* **84**, 011151 (2011).
- [19] S. Bedkihal, M. Bandyopadhyay, and D. Segal, *The European Physical Journal B* **86**, 506 (2013).
- [20] J. L. D'Amato and H. M. Pastawski, *Phys. Rev. B* **41**, 7411 (1990).
- [21] D. Roy, *Journal of Physics: Condensed Matter* **20**, 025206 (2007).
- [22] D. Roy and A. Dhar, *Phys. Rev. B* **75**, 195110 (2007).
- [23] E. Zerah-Harush and Y. Dubi, *Phys. Rev. Research* **2**, 023294 (2020).
- [24] M. Kulkarni, K. L. Tiwari, and D. Segal, *New Journal of Physics* **15**, 013014 (2013).
- [25] M. Kulkarni, K. L. Tiwari, and D. Segal, *Phys. Rev. B* **86**, 155424 (2012).
- [26] M. Saha, B. K. Agarwalla, M. Kulkarni, and A. Purkayastha, (2022), [arXiv:2205.02214 \[quant-ph\]](https://arxiv.org/abs/2205.02214).
- [27] Y. Last, *Communications in Mathematical Physics* **151**, 183 (1993).
- [28] L. Molinari, *Journal of Physics A: Mathematical and General* **30**, 983 (1997).
- [29] L. Molinari, *Journal of Physics A: Mathematical and General* **31**, 8553 (1998).
- [30] M. Žnidarič and M. Horvat, *The European Physical Journal B* **86**, 67 (2013).

- [31] M. V. Medvedyeva, T. c. v. Prosen, and M. Žnidarič, *Phys. Rev. B* **93**, 094205 (2016).
- [32] M. Žnidarič, J. J. Mendoza-Arenas, S. R. Clark, and J. Goold, *Annalen der Physik* **529**, 1600298 (2017).
- [33] M. Žnidarič, *Phys. Rev. B* **97**, 214202 (2018).
- [34] A. M. Lacerda, J. Goold, and G. T. Landi, *Phys. Rev. B* **104**, 174203 (2021).
- [35] D. Dwiputra and F. P. Zen, *Phys. Rev. A* **104**, 022205 (2021).
- [36] C. Chiaracane, A. Purkayastha, M. T. Mitchison, and J. Goold, *Phys. Rev. B* **105**, 134203 (2022).
- [37] X. Turkeshi and M. Schiró, *Phys. Rev. B* **104**, 144301 (2021).
- [38] R. Krishna Kumar, D. A. Bandurin, F. M. D. Pellegrino, Y. Cao, A. Principi, H. Guo, G. H. Auton, M. Ben Shalom, L. A. Ponomarenko, G. Falkovich, K. Watanabe, T. Taniguchi, I. V. Grigorieva, L. S. Levitov, M. Polini, and A. K. Geim, *Nature Physics* **13**, 1182 (2017).
- [39] O. E. Raichev, (2022), [arXiv:2202.06623](https://arxiv.org/abs/2202.06623) [cond-mat.mes-hall].
- [40] L. V. Ginzburg, C. Gold, M. P. Rössli, C. Reichl, M. Berl, W. Wegscheider, T. Ihn, and K. Ensslin, *Phys. Rev. Research* **3**, 023033 (2021).
- [41] A. Szameit, S. Stützer, T. Kottos, A. Tünnermann, S. Nolte, and D. N. Christodoulides, *Frontiers in Optics 2012/Laser Science XXVIII*, FTh2G.1 (2012).
- [42] S. Stützer, T. Kottos, A. Tünnermann, S. Nolte, D. N. Christodoulides, and A. Szameit, *2013 Conference on Lasers and Electro-Optics - International Quantum Electronics Conference* (2013).
- [43] S. Stützer, T. Kottos, A. Tünnermann, S. Nolte, D. N. Christodoulides, and A. Szameit, *Conference on Lasers and Electro-Optics 2012* (2012).
- [44] Supplemental Material.
- [45] M. Saha, B. P. Venkatesh, and B. K. Agarwalla, *Phys. Rev. B* **105**, 224204 (2022).
- [46] N. Sergueev, D. Roubtsov, and H. Guo, *Phys. Rev. Lett.* **95**, 146803 (2005).
- [47] H. M. Pastawski, L. Foa Torres, and E. Medina, *Chemical Physics* **281**, 257 (2002).
- [48] H. Haug and A. Jauho, *Quantum Kinetics in Transport and Optics of Semiconductors* (Springer, New York, 2008).

SUPPLEMENTARY MATERIAL

S1. BÜTTIKER VOLTAGE PROBE

In this section, we lay out some details about Büttiker voltage probe and its specific implementation in our case. Our entire setup that includes the finite tight-binding chain, the left/right reservoirs and the probes, are all of bilinear type. As a consequence, the non-equilibrium steady state electronic current (NESS) flowing out of each terminal follows the Landauer formula [48],

$$\mathcal{I}_\nu = \sum_\alpha \int_{-\infty}^{\infty} \mathcal{T}_{\nu\alpha}(\omega) \left(f_\nu(\omega) - f_\alpha(\omega) \right) d\omega. \quad (\text{S1})$$

Here $f_\nu(\omega) = (1 + e^{\beta(\omega - \mu_\nu)})^{-1}$ is the Fermi distribution function of ν -th terminal with inverse temperature β and chemical potential μ_ν (same for $f_\alpha(\omega)$ with chemical potential μ_α). $\mathcal{T}_{\nu\alpha}(\omega) = \text{Tr}[\Gamma_\nu(\omega)G^r(\omega)\Gamma_\alpha(\omega)G^a(\omega)]$ is the transmission probability for electrons to flow from α -th terminal to ν -th terminal. Here $G^r(\omega)$ is the retarded Green's function of the lattice chain in presence of the reservoirs. For sake of brevity, we suppress the superscript r and denote the retarded Green's function as $G(\omega)$ given by

$$G(\omega) = [\omega\mathbb{I} - H_C - \Sigma_L(\omega) - \Sigma_R(\omega) - \sum_{n=1}^N \Sigma_{P_n}(\omega)]^{-1}. \quad (\text{S2})$$

Here \mathbb{I} being the $N \times N$ identity matrix and H_C represents the single particle Hamiltonian corresponding to \hat{H}_C . The advanced Green's function is given by $G^a(\omega) = G^\dagger(\omega)$. $\Sigma_L(\omega), \Sigma_R(\omega)$ are the self-energy matrices for the left and right reservoirs, respectively. $\Sigma_{P_n}(\omega)$ is the self-energy of the n -th probe. The hybridization matrix is obtained as $\Gamma_\alpha(\omega) = -2\text{Im}[\Sigma_\alpha(\omega)]$ where $\alpha = L, R, P$. For simplicity, we approximate the self energy terms by the wide-band limit, i.e., $\Sigma_L(\omega)|_{11} = -i\tau/2$, $\Sigma_R(\omega)|_{NN} = -i\tau/2$, and $\Sigma_{P_n}|_{nn} = -i\tau_p/2$.

Following the Büttiker probe technique, different types of incoherent effects can be realized. For example, at a given voltage bias between the left and the right reservoirs and uniform finite temperature at all terminals, incoherent elastic scattering processes can be implemented by demanding frequency resolved zero charge and energy current between each probe and the system. Such probes are often referred to as dephasing probes. On the other hand, incoherent inelastic processes can be implemented via the so-called voltage probe technique where the net charge current flowing between each probe and the system vanishes whereas the energy current remains finite.

Since in our work, we focus on electronic conductance, we consider a linear response regime by assuming small chemical potential difference between the left and the right reservoir. The chemical potential for the probes are determined by the zero electronic current conditions. We expand the Fermi-distribution functions in Eq. (S1)

as

$$\begin{aligned} f_\nu(\omega) &= f_{\text{eq}}(\omega) - \left. \frac{\partial f_{\text{eq}}(\omega)}{\partial \omega} \right|_{\epsilon_F} (\mu_\nu - \epsilon_F) \\ f_\alpha(\omega) &= f_{\text{eq}}(\omega) - \left. \frac{\partial f_{\text{eq}}(\omega)}{\partial \omega} \right|_{\epsilon_F} (\mu_\alpha - \epsilon_F), \end{aligned} \quad (\text{S3})$$

where ϵ_F is the chosen chemical potential at equilibrium. Now putting Eq. (S3) in Eq. (S1), we get an expression for the electronic current flowing out of the n -th probe as

$$\begin{aligned} \mathcal{I}_n &= \sum_\alpha \int_{-\infty}^{\infty} \mathcal{T}_{n\alpha}(\omega) \left(-\frac{\partial f_{\text{eq}}(\omega)}{\partial \omega} \right) (\mu_n - \mu_\alpha) d\omega \\ &= \left[\mu_n \sum_\alpha \int_{-\infty}^{\infty} \mathcal{T}_{n\alpha}(\omega) \left(-\frac{\partial f_{\text{eq}}(\omega)}{\partial \omega} \right) d\omega \right. \\ &\quad - \sum_{n'=1}^N \mu_{n'} \int_{-\infty}^{\infty} \mathcal{T}_{nn'}(\omega) \left(-\frac{\partial f_{\text{eq}}(\omega)}{\partial \omega} \right) d\omega \\ &\quad - \mu_L \int_{-\infty}^{\infty} \mathcal{T}_{nL}(\omega) \left(-\frac{\partial f_{\text{eq}}(\omega)}{\partial \omega} \right) d\omega \\ &\quad \left. - \mu_R \int_{-\infty}^{\infty} \mathcal{T}_{nR}(\omega) \left(-\frac{\partial f_{\text{eq}}(\omega)}{\partial \omega} \right) d\omega \right]. \end{aligned} \quad (\text{S4})$$

The voltage probe condition demands $\mathcal{I}_n = 0$ for each $n = 1, 2, \dots, N$ leading to N linear equations which after solving yields unique probe chemical potentials. This analysis further simplifies Eq. (S4) in the zero temperature limit ($\beta \rightarrow \infty$) to yield

$$\begin{aligned} \mu_n \sum_\alpha \mathcal{T}_{n\alpha}(\epsilon_F) - \sum_{n'=1}^N \mu_{n'} \mathcal{T}_{nn'}(\epsilon_F) \\ = \mu_L \mathcal{T}_{nL}(\epsilon_F) + \mu_R \mathcal{T}_{nR}(\epsilon_F). \end{aligned} \quad (\text{S5})$$

A more compact way of expressing the above equation is

$$\begin{aligned} (\mu_n - \mu_R) \sum_\alpha \mathcal{T}_{n\alpha}(\epsilon_F) - \sum_{n'=1}^N (\mu_{n'} - \mu_R) \mathcal{T}_{nn'}(\epsilon_F) \\ = (\mu_L - \mu_R) \mathcal{T}_{nL}(\epsilon_F). \end{aligned} \quad (\text{S6})$$

From Eq. (S6) putting the transmission probabilities explicitly in terms of NEGF, we can write down the solution for chemical potential of each probe n as,

$$\begin{aligned} \mu_n = \mu_R + \tau \sum_{j=1}^N \mathcal{W}_{nj}^{-1}(\epsilon_F) |G_{j1}(\epsilon_F)|^2 (\mu_L - \mu_R) \\ \forall n = 1, 2, 3, \dots, N \end{aligned} \quad (\text{S7})$$

Here, the elements of the $N \times N$ matrix $\mathcal{W}(\epsilon_F)$ are

$$\begin{aligned} \mathcal{W}_{nj} &= -\tau_p |G_{nj}|^2, \quad \forall n \neq j \\ \mathcal{W}_{nn} &= \tau (|G_{n1}|^2 + |G_{nN}|^2) + \tau_p \sum_{j \neq n} |G_{nj}|^2, \end{aligned} \quad (\text{S8})$$

We consider $\mu_R = \epsilon_F$, $\mu_L = \epsilon_F + \delta\mu$ and $\mu_n = \epsilon_F + \delta\mu_n$. By determining the probe chemical potentials μ_n using Eq. (S7), one can find the two-terminal electronic conductance, defined as, $\mathcal{G}(\epsilon_F) = \mathcal{I}_L/\delta\mu$ where \mathcal{I}_L is given in Eq. (S1). The conductance is given by [20],

$$\begin{aligned} \mathcal{G}(\epsilon_F) &= \tau^2 |G_{1N}(\epsilon_F)|^2 \\ &+ \tau^2 \tau_p \sum_{n,j=1}^N |G_{Nn}(\epsilon_F)|^2 \mathcal{W}_{nj}^{-1}(\epsilon_F) |G_{j1}(\epsilon_F)|^2 \end{aligned} \quad (\text{S9})$$

which was given in the main text.

S2. DETAILS ABOUT PERTURBATIVE EXPANSION OF \mathcal{W} UPTO $\mathcal{O}(\tau_p)$

In this section, we provide details about the perturbative expansion of \mathcal{W} upto $\mathcal{O}(\tau_p)$. We write \mathcal{W} as,

$$\mathcal{W}_{lm} = \mathcal{W}_{lm}^{(1)} + \tau_p \mathcal{W}_{lm}^{(2)} + \mathcal{O}(\tau_p^2). \quad (\text{S10})$$

We now get the components of \mathcal{W} by performing the perturbative expansion in NEGF, as given in Eq. (S2).

$$\mathcal{W}_{lm}^{(2)} = \begin{cases} -|G_{lm}^0|^2, & \forall l \neq m \\ \sum_{\alpha=1}^N |G_{l\alpha}^0|^2 + \frac{i\tau}{2} \left[G_{lN}^0 (G^{0a} G^{0a})_{Nl} + G_{l1}^0 (G^{0a} G^{0a})_{1l} - G_{Nl}^{0a} (G^0 G^0)_{lN} - G_{1l}^{0a} (G^0 G^0)_{1l} \right], & \forall l = m \end{cases} \quad (\text{S15})$$

To check the validity of our approximation upto $\mathcal{O}(\tau_p)$ in \mathcal{W} , we have computed the two-terminal conductance using three different methods:

Method 1: We keep terms up to $\mathcal{O}(\tau_p)$ in both \mathcal{W} and in the NEGF which appears in the second term of two-terminal conductance in presence of probes [see Eq. (S9)].

Upto $\mathcal{O}(\tau_p)$ we get

$$\begin{aligned} G(\omega) &= \left[\omega \mathbb{I} - H_S - \Sigma_L - \Sigma_R - \sum_{n=1}^N \Sigma_{P_n} \right]^{-1} \\ &= \left[(G^0)^{-1} - \sum_{n=1}^N \Sigma_{P_n} \right]^{-1} \\ &= \left[(G^0)^{-1} + \frac{i\tau_p}{2} \mathbb{I} \right]^{-1} \\ &= G^0 - \frac{i\tau_p}{2} G^0 G^0 + \mathcal{O}(\tau_p^2) \end{aligned} \quad (\text{S11})$$

where recall that G^0 is the retarded Green's function in absence of the probes. We have suppressed the argument ω for sake of brevity. As we are interested upto τ_p terms, following Eq. (S11), the off-diagonal term ($l \neq m$) of \mathcal{W} can be simply replaced by $-\tau_p |G_{lm}^0|^2$. Similarly, the second term in the the diagonal piece ($l = m$) of \mathcal{W} , given in Eq. (S8), can be replaced by $\tau_p \sum_{\alpha=1}^N |G_{l\alpha}^0|^2$. The term proportional to τ in Eq. (S8) needs to be carefully analyzed. For this purpose, an expansion in τ_p for $|G_{l1}|^2$ is carried out and is given by,

$$\begin{aligned} |G_{l1}|^2 &= |G_{l1}^0|^2 \\ &- \frac{i\tau_p}{2} \left[G_{1l}^{0a} (G^0 G^0)_{1l} - G_{l1}^0 (G^{0a} G^{0a})_{1l} \right] + \mathcal{O}(\tau_p^2), \end{aligned} \quad (\text{S12})$$

where G^{0a} is the advanced Green's function without the probes. In a similar fashion,

$$\begin{aligned} |G_{lN}|^2 &= |G_{lN}^0|^2 \\ &- \frac{i\tau_p}{2} \left[G_{Nl}^{0a} (G^0 G^0)_{lN} - G_{lN}^0 (G^{0a} G^{0a})_{Nl} \right] + \mathcal{O}(\tau_p^2). \end{aligned} \quad (\text{S13})$$

As a result, Eq. (S8), up to $\mathcal{O}(\tau_p)$, is given as,

$$\mathcal{W}_{lm}^{(1)} = \begin{cases} 0, & \forall l \neq m \\ \tau \left(|G_{l1}^0|^2 + |G_{lN}^0|^2 \right), & \forall l = m \end{cases} \quad (\text{S14})$$

and

NEGF's up to $\mathcal{O}(\tau_p)$ are

$$\begin{aligned} |G_{Nn}|^2 &= |G_{Nn}^0|^2 \\ &+ i \frac{\tau_p}{2} \left[G_{Nn}^0 (G^{0a} G^{0a})_{nN} - G_{nN}^{0a} (G^0 G^0)_{Nn} \right], \\ |G_{j1}|^2 &= |G_{j1}^0|^2 \\ &+ i \frac{\tau_p}{2} \left[G_{j1}^0 (G^{0a} G^{0a})_{1j} - G_{1j}^{0a} (G^0 G^0)_{j1} \right]. \end{aligned} \quad (\text{S16})$$

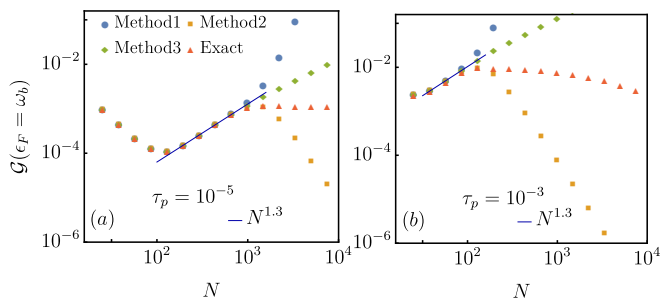


FIG. S1. (Color online): Plot for conductance in presence of Büttiker probes at the band edge ($\epsilon_F = \omega_b$). The exact result is compared with three different perturbative methods, as mentioned in the text. The probe couplings are (a) $\tau_p = 10^{-5}$ and (b) $\tau_p = 10^{-3}$. The superballistic regime is perfectly captured by all the three methods. The deviation from the exact result occur just after the termination of the superballistic regime.

Method 2: We keep terms up to $\mathcal{O}(\tau_p)$ in \mathcal{W} but for the NEGFs we keep τ_p independent terms which are given by,

$$\begin{aligned} |G_{Nn}|^2 &= |G_{Nn}^0|^2, \\ |G_{j1}|^2 &= |G_{j1}^0|^2. \end{aligned} \quad (\text{S17})$$

Method 3: We approximate exact expression for \mathcal{W} [see Eq. (S8)] by replacing the NEGF G by G^0 and also for the NEGF's in Eq. (S9). As a result the NEGFs have the form same as in method 2, whereas the form of \mathcal{W} is given by,

$$\mathcal{W}_{lm} = \begin{cases} -\tau_p |G_{lm}^0|^2, & \forall l \neq m \\ \tau(|G_{l1}^0|^2 + |G_{lN}^0|^2) + \tau_p \sum_{\alpha=1}^N |G_{l\alpha}^0|^2, & \forall l = m. \end{cases} \quad (\text{S18})$$

Remarkably, all the above three methods perfectly capture the superballistic transport regime for conductance with system length N . In Fig. S1, we display the conductance at the band edge obtained from the three methods. We see a clear evidence of the SB transport regime captured by all the methods and matches perfectly with the exact numerics. However beyond the SB regime, all the above mentioned perturbative approximations fail to capture the exact trend in conductance.

S3. VALIDITY OF DIFFERENT PERTURBATIVE METHODS OUTSIDE AND WITHIN THE BAND EDGE

In this section, we consider the scenario when the chemical potential is located either outside or within the band edge. We show the comparison between the results obtained following the different perturbative methods and the exact numerics for the electronic conductance for both weak and strong probe coupling strengths. Fig. S2 (a) and (b) shows that all the three perturbative

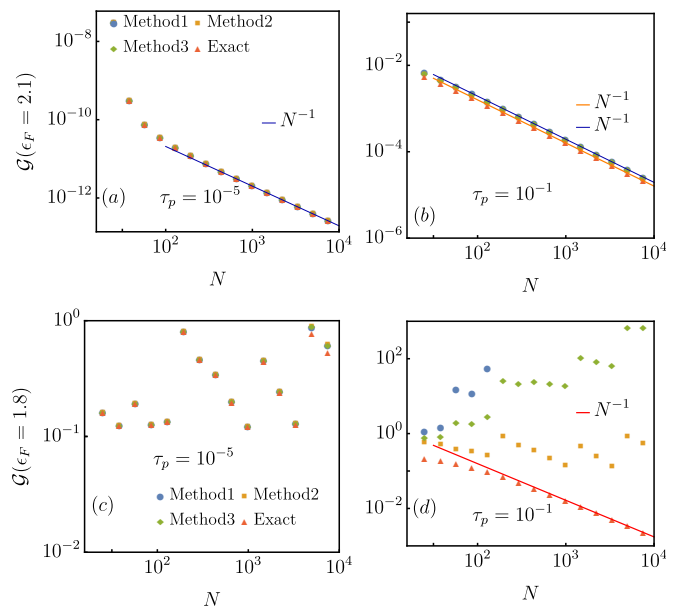


FIG. S2. (Color online): Plot for conductance outside ($\epsilon_F = 2.1$) [(a) and (b)] and inside ($\epsilon_F = 1.8$) of the band edge [(c) and (d)] for two different probe couplings $\tau_p = 10^{-5}$ and $\tau_p = 10^{-1}$, respectively. For weak probe coupling [(a) and (c)], all the three methods agree irrespective of whether the ϵ_F is inside or outside the band edge. In contrast, for strong probe coupling [(b) and (d)], the perturbative results differ from the exact numerics. Interestingly, for $\epsilon_F = 2.1$, (b) all three methods correctly capture the diffusive behaviour. In contrast, for $\epsilon_F = 1.8$, at strong coupling (d) all the three methods fail to capture the diffusive behaviour in conductance.

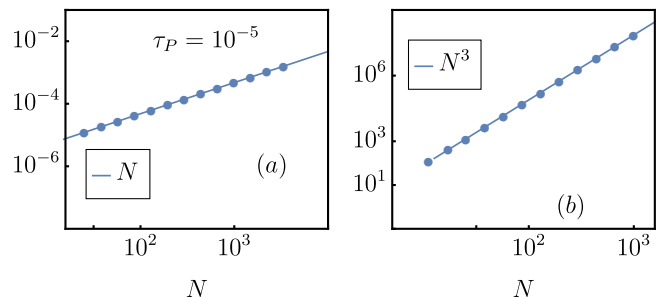


FIG. S3. (Color online): Plot for (a) Eq. (S20), and (b) $\sum_{n=1}^N f(n)$ as a function of N at the band edge.

methods perfectly capture the crossover from exponentially suppressed to diffusive transport when the chemical potential is lying outside the band edge ($\epsilon_F = 2.1$). In the other scenario, i.e, within the band edge ($\epsilon_F = 1.8$) [Fig. S2 (c) and (d)] results for conductance perfectly match with exact numerics for weak coupling with all three methods. However, for strong coupling all three perturbative methods fail to capture the diffusive trend predicted by exact calculations. This analysis shows that the specific perturbative methods studied in this

work are not suitable for capturing ballistic to diffusive crossover. Remarkably, at and outside the band edge, the perturbative methods are highly efficient in predicting the crossover in transport features.

S4. LINEAR N SCALING IN CONDUCTANCE – UNDERSTANDING THE ONSET OF SUPERBALLISTIC TRANSPORT

In this section, we are interested to find the scaling of conductance with system size. We focus on the conductance expression that is valid upto the linear order in τ_p , given as

$$\mathcal{G}(\epsilon_F) = \tau^2 |G_{1N}^0(\epsilon_F)|^2 \quad (\text{S19})$$

$$+ \tau \tau_p \sum_{n=1}^N \frac{|G_{Nn}^0(\epsilon_F)|^2 |G_{n1}^0(\epsilon_F)|^2}{|G_{n1}^0(\epsilon_F)|^2 + |G_{Nn}^0(\epsilon_F)|^2} + \mathcal{O}(\tau_p^2).$$

Note that, at the band edge, the first term provides a subdiffusive $1/N^2$ scaling in conductance [26]. We therefore focus on the second term

$$\tau \tau_p \sum_{n=1}^N \frac{|G_{Nn}^0(\epsilon_F)|^2 |G_{n1}^0(\epsilon_F)|^2}{|G_{n1}^0(\epsilon_F)|^2 + |G_{Nn}^0(\epsilon_F)|^2} \quad (\text{S20})$$

and analyze the system size N dependence. Recall that, G^0 is the NEGF matrix for the system in absence of probes. As the single-particle Hamiltonian of the system is tridiagonal, the NEGF in this case can be solved exactly, and given as,

$$G_{\ell j}^0(\omega) = (-1)^{\ell+j} \frac{\Delta_{1,\ell-1}(\omega) \Delta_{N-j,N}(\omega)}{\Delta_{1,N}(\omega)}, \quad (\text{S21})$$

where $\Delta_{i,j}(\omega)$ is the determinant of a part of the matrix $\mathcal{M}(\omega)$, given as

$$\mathcal{M}(\omega) = \begin{pmatrix} \omega - \Sigma_L|_{1,1} & 1 & 0 & 0 & \dots \\ 1 & \omega & 1 & 0 & \dots \\ 0 & 1 & \omega & 1 & \dots \\ \dots & \dots & \dots & \dots & \dots \\ 0 & 0 & 0 & 1 & \omega - \Sigma_R|_{N,N} \end{pmatrix}. \quad (\text{S22})$$

The part of the matrix of $\mathcal{M}(\omega)$ is constructed by starting from i -th row and column and ending with j -th row and column. Note that, albeit we use the same notation $\Delta_{i,j}(\omega)$ as in main text, here we are using it in the context of Green's function in absence of probes. The determinants $\Delta_{1,N}(\omega)$, $\Delta_{1,\ell-1}(\omega)$ and $\Delta_{N-p,N}(\omega)$ that appears in Eq. (S21) can be computed following the transfer matrix approach [26]. The equations which solve the deter-

minants are following,

$$\begin{pmatrix} \Delta_{1,N} \\ \Delta_{1,N-1} \end{pmatrix} = \begin{pmatrix} 1 & -\Sigma_L|_{1,1} \\ 0 & 1 \end{pmatrix} \begin{pmatrix} \omega & -1 \\ 1 & 0 \end{pmatrix}^N \begin{pmatrix} 1 \\ \Sigma_R|_{N,N} \end{pmatrix},$$

$$\begin{pmatrix} \Delta_{1,\ell-1} \\ \Delta_{1,\ell-2} \end{pmatrix} = \begin{pmatrix} 1 & -\Sigma_L|_{1,1} \\ 0 & 1 \end{pmatrix} \begin{pmatrix} \omega & -1 \\ 1 & 0 \end{pmatrix}^{\ell-1} \begin{pmatrix} 1 \\ 0 \end{pmatrix}, \quad (\text{S23})$$

$$\begin{pmatrix} \Delta_{N-p,N} \\ \Delta_{N-p-1,N} \end{pmatrix} = \begin{pmatrix} \omega & -1 \\ 1 & 0 \end{pmatrix}^{N-p} \begin{pmatrix} 1 \\ \Sigma_R|_{N,N} \end{pmatrix}.$$

At the band edges $\omega_b = \pm 2$, the transfer matrix is non-diagonalizable and has exceptional points. However, one can write the matrix in the Jordan-normal form $\begin{pmatrix} 1 & 1 \\ 0 & 1 \end{pmatrix}$ by using a transformation $S = \begin{pmatrix} i & 0 \\ i & -i \end{pmatrix}$. With these in hand, we get the specific forms of the determinants, given as

$$\Delta_{1,N}(\omega_b) = \frac{3N+5}{4} + iN,$$

$$\Delta_{1,\ell-1}(\omega_b) = \ell + i \left(\frac{\ell-1}{2} \right), \quad (\text{S24})$$

$$\Delta_{N-p,N}(\omega_b) = (N-p+1) + i \left(\frac{N-p}{2} \right).$$

Finally using Eq. (S20), we get

$$\tau \tau_p \sum_{n=1}^N \frac{|G_{Nn}^0(\omega_b)|^2 |G_{n1}^0(\omega_b)|^2}{|G_{n1}^0(\omega_b)|^2 + |G_{Nn}^0(\omega_b)|^2}$$

$$= \frac{\tau \tau_p}{|\Delta_{1,N}(\omega_b)|^2} \sum_{n=1}^N f(n) \propto N, \quad (\text{S25})$$

where $f(n)$ is given by

$$f(n) = \frac{|\Delta_{1,n-1}(\omega_b)|^2 |\Delta_{N-n,N}(\omega_b)|^2}{|\Delta_{1,n-1}(\omega_b)|^2 + |\Delta_{N-n,N}(\omega_b)|^2}. \quad (\text{S26})$$

We find that

$$\sum_{n=1}^N f(n) \propto N^3 \quad (\text{S27})$$

and is clearly shown in Fig. S3(b). Also from Eq. (S24) we find

$$|\Delta_{1,N}(\omega_b)|^2 \propto N^2. \quad (\text{S28})$$

As a result, upto the linear order in τ_p , the second term in the conductance in Eq. (S19) scales linearly with N at the band-edge, as shown in Fig. S3(a). This term is therefore responsible for the onset of the superballistic transport regime.

S5. PARTICLE DENSITY IN THE ABSENCE AND THE PRESENCE OF PROBES

In this section, we show that the effect of having voltage probes is very different from the effect of having

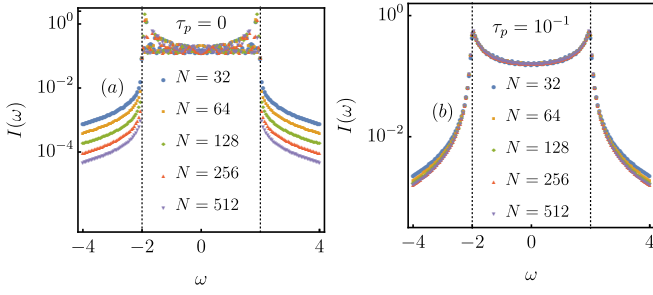


FIG. S4. (Color online): We plot integrand $I(\omega)$, defined in Eq. (S31), of the particle density as a function of ω for different N with weak to strong probe couplings.

many-body interactions in the system, although both are sources of inelastic scattering. To this end, we calculate the particle density of the system which is defined by,

$$\gamma = \frac{1}{N} \sum_{\ell=1}^N \langle c_{\ell}^{\dagger} c_{\ell} \rangle. \quad (\text{S29})$$

At equilibrium, the occupation at the ℓ th site in presence of probes can be written as,

$$\begin{aligned} \langle c_{\ell}^{\dagger} c_{\ell} \rangle &= \tau \int_{-\infty}^{\epsilon_F} (|G_{1\ell}(\omega)|^2 + |G_{N\ell}(\omega)|^2) \frac{d\omega}{2\pi} \\ &+ \tau_p \int_{-\infty}^{\epsilon_F} \sum_{\alpha=1}^N |G_{\alpha\ell}(\omega)|^2 \frac{d\omega}{2\pi} \end{aligned} \quad (\text{S30})$$

where we recall that ϵ_F is the Fermi energy. Thus, the full integrand in the particle density is

$$\begin{aligned} I(\omega) &= \frac{1}{2\pi N} \sum_{\ell=1}^N \left[\tau (|G_{1\ell}(\omega)|^2 + |G_{N\ell}(\omega)|^2) \right. \\ &\left. + \tau_p \sum_{\alpha=1}^N |G_{\alpha\ell}(\omega)|^2 \right] \end{aligned} \quad (\text{S31})$$

and therefore

$$\gamma = \int_{-\infty}^{\epsilon_F} I(\omega) d\omega. \quad (\text{S32})$$

To conclude about the N dependence of γ , we plot $I(\omega)$ for different system lengths N . In absence of probes, i.e., $\tau_p = 0$, we see in Fig. S4(a) that $I(\omega)$ decreases with N for $\omega \leq -2$, i.e., ω below lower band-edge. This means particle density at lower band-edge, i.e., γ for $\epsilon_F = -2$, decreases with N . Thus, as system-size increases, the particle density goes to zero. As a consequence of vanishing particle density at large system length, the transport mechanism is governed by the single-particle sector. So, even if number conserving many-body interactions are

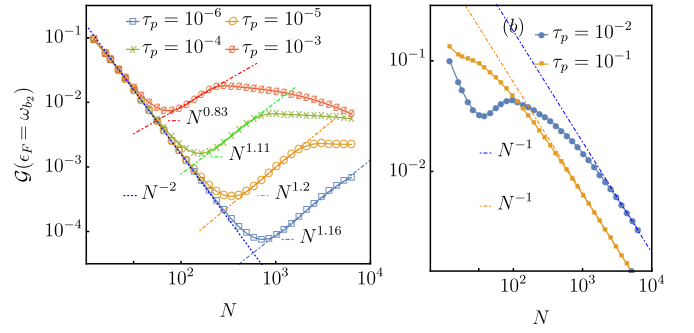


FIG. S5. (Color online):(a) Behavior of conductance at one of the band-edges $\epsilon_F = \omega_{b_2} = -W$ of a two-band model given in Eq. (S39) vs system size for small τ_p . The sub-diffusive to superballistic crossover is clearly seen. (b) Plots of conductance at larger values of τ_p which captures the eventual crossover to conventional diffusive regime at large N . All the other band-edges show similar behavior. Here we choose $W = 0.5$.

switched on within the lattice chain, it will have a negligible effect. Consequently, the sub-diffusive behavior, that is seen at the band edges in absence of many-body interactions, survives even in presence of interactions.

In Fig. S4(b) we plot $I(\omega)$ for different system lengths N for $\tau_p = 0.1$. We clearly see that on increasing system-size, $I(\omega)$ collapses to a single curve. This means particle density at lower band-edge, i.e., γ for $\epsilon_F = -2$ saturates with increasing N . Thus, contrary to the situation in absence of probes, in presence of probes there is finite particle density at large N for $\epsilon_F = -2$. So, even though having many-body interactions (in the system) or the presence of probes are sources of inelastic scattering, they have remarkably different effect at the lower band-edge. Similar conclusion can be reached for the upper band-edge, $\epsilon_F = 2$, when considering holes instead of particles.

S6. EIGENVALUES OF $\mathbf{T}(\omega)$ AND NEGF IN PRESENCE OF PROBES

The matrix $\mathbf{T}(\omega)$ of a normal tight-binding model in presence of probes is given by,

$$\mathbf{T}(\omega) = \mathbf{T}^0(\omega) + \frac{i\tau_p}{4} (\mathbb{I}_2 + \sigma_z) \quad (\text{S33})$$

Here $\mathbf{T}^0(\omega) = \frac{\omega}{2} (\mathbb{I}_2 + \sigma_z) - i\sigma_y$. Thus, $\mathbf{T}(\omega) = (\frac{\omega}{2} + \frac{i\tau_p}{4}) (\mathbb{I}_2 + \sigma_z) - i\sigma_y$. The eigenvalues of $\mathbf{T}(\omega)$ is,

$$\lambda_{\pm} = \frac{1}{2} \left[\omega + \frac{i\tau_p}{2} \pm \sqrt{\left(\omega + \frac{i\tau_p}{2} \right)^2 - 4} \right] \quad (\text{S34})$$

This can be written as, $\lambda_{\pm} = e^{\pm(\kappa_1 + i\kappa_2)}$, with $\kappa_1, \kappa_2 \geq 0$ and $\kappa_1 = \log|\lambda_{+}|$.

A. NEGF in presence of probes for all ω

It can be checked that with $\tau_p > 0$ for all ω , in Eq. (S34), absolute value of one of the eigenvalues $|\lambda_+|$ is greater than 1, while the other $|\lambda_-|$ is less than 1. It ensures that $\kappa_1 > 0$. For the NEGF, we know that

$$|G_{\ell j}(\omega)|^2 = \frac{|\Delta_{1,\ell-1}(\omega)|^2 |\Delta_{N-j,N}(\omega)|^2}{|\Delta_{1,N}(\omega)|^2}. \quad (\text{S35})$$

Since the determinant $\Delta_{i,j}$ is related to $\mathbf{T}(\omega)$, calculating it requires calculating powers of $\mathbf{T}(\omega)$. The value of $\Delta_{i,j}$ is therefore dominated by the eigenvalue with larger magnitude, i.e., λ_+ . So, we find that, $|\Delta_{1,\ell-1}(\omega)|^2 \sim e^{2\kappa_1 \ell}$, $|\Delta_{N-j,N}(\omega)|^2 \sim e^{2\kappa_1(N-j)}$ and $|\Delta_{1,N}(\omega)|^2 \sim e^{2\kappa_1 N}$. Putting all these values in Eq. (S35), we get $|G_{\ell j}(\omega)|^2 \sim e^{-2\kappa_1|\ell-j|}$. Thus, if we write $|G_{\ell j}(\omega)|^2 \sim e^{-|\ell-j|/\xi}$, (ξ is the localization length), then $\xi^{-1} = 2\kappa_1$.

B. Small τ_p behaviour of $|\lambda_{\pm}|$ at the band edges

The eigenvalues of $\mathbf{T}(\omega)$ at one of the band edges $\omega_b = 2$ reduces to,

$$\begin{aligned} \lambda_{\pm} &= \frac{1}{2} \left[2 + \frac{i\tau_p}{2} \pm \sqrt{\left(-\frac{\tau_p^2}{4} + 2i\tau_p\right)} \right] \\ &= 1 + \frac{i\tau_p}{4} \pm \sqrt{\tau_p} \sqrt{-\frac{\tau_p}{16} + \frac{i}{2}}. \end{aligned} \quad (\text{S36})$$

Defining $\theta = \tan^{-1}(8/\tau_p)$, we can write the above equation as,

$$\begin{aligned} \lambda_{\pm} &= 1 + \frac{i\tau_p}{4} \pm \sqrt{\tau_p} \exp(-i\theta/2) \\ &= 1 \pm \sqrt{\tau_p} \cos(\theta/2) + \frac{i\tau_p}{4} \mp i\sqrt{\tau_p} \sin(\theta/2), \end{aligned} \quad (\text{S37})$$

where $\cos(\theta) = \frac{\tau_p}{\sqrt{64+\tau_p^2}}$ and $\sin(\theta) = \frac{8}{\sqrt{64+\tau_p^2}}$. Taking the absolute value of Eq. (S37) we obtain

$$\begin{aligned} |\lambda_{\pm}| &= \sqrt{\left(1 \pm \sqrt{\tau_p} \cos(\theta/2)\right)^2 + \left(\frac{\tau_p}{4} \mp \sqrt{\tau_p} \sin(\theta/2)\right)^2} \\ &= \sqrt{1 + \tau_p + \frac{\tau_p^2}{16} \pm 2\sqrt{\tau_p} \cos(\theta/2) \mp \frac{\tau_p^{3/2}}{2} \sin(\theta/2)} \\ &\approx \sqrt{1 \pm 2\sqrt{\tau_p}} \quad \text{small } \tau_p \\ &\approx 1 \pm \sqrt{\tau_p}. \end{aligned} \quad (\text{S38})$$

Exactly same result can be obtained for the lower band edge, $\omega_b = -2$ as well.

S7. SUPERBALLISTIC SCALING OF CONDUCTANCE AT THE BAND EDGES OF TWO-BAND MODEL

In this section, we discuss the situation when the tight-binding lattice supports two bands. Let us consider the

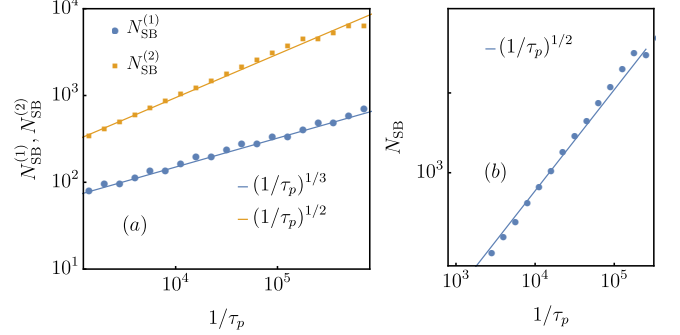


FIG. S6. (Color online): (a) The scaling of the system-size corresponding to the start (end) of the superballistic scaling regime $N_{\text{SB}}^{(1)}$ ($N_{\text{SB}}^{(2)}$) with τ_p^{-1} for the two-band model given in Eq. (S39). (b) The scaling of the size of the superballistic scaling regime $N_{\text{SB}} = N_{\text{SB}}^{(2)} - N_{\text{SB}}^{(1)}$ with $1/\tau_p$. This clearly shows that the superballistic scaling regime expands on decreasing τ_p .

periodic onsite potential term as

$$V = \sum_{i=1}^N \epsilon_i c_i^\dagger c_i = W \sum_{i=1}^N \cos[2\pi b i] c_i^\dagger c_i \quad (\text{S39})$$

with the usual nearest neighbour hopping term discussed in the main text. Here i is the site index, W is the strength of the onsite potential and we choose $b = 1/2$ i.e., the two band case. The unit cell transfer matrix without the probes for this case is,

$$\mathbf{T}^0(\omega) = \prod_{j=1}^2 \mathbf{T}^{0(j)}(\omega) \quad (\text{S40})$$

with

$$\mathbf{T}^{0(j)}(\omega) = \frac{\omega - \epsilon_j}{2} (\mathbb{I}_2 + \sigma_z) - i\sigma_y. \quad (\text{S41})$$

Here $\mathbf{T}^{0(j)}(\omega)$ is the transfer matrix for the each site j . At the band edges of the two-band case ($\omega = \omega_{b_2}$),

$$\text{Tr}[\mathbf{T}^0(\omega = \omega_{b_2})] = \pm 2. \quad (\text{S42})$$

The subscript b_2 in ω_{b_2} indicates the fact that we are considering the two-band case. Solving the above condition [Eq. (S42)], one will get four band edges at the values, $\omega_{b_2} = \pm W, \pm\sqrt{4+W^2}$. Now, in presence of weak environment effects, we show the superballistic behaviour for one of the band edges $\omega_{b_2} = -W$ of two-band model in Fig. S5 (a). With increasing probe strength, the crossover from superballistic to diffusive regime is also visible in Fig. S5 (b). The superballistic regime also can be expanded like the one-band model which we have shown in Fig. S6. These findings hold for any chosen band edge and is generalisable to chains that host more than two bands.